Jibin Tian
Key Laboratory for Thermal Science and Power Engineering of Ministry of Education, Beijing Key Laboratory of CO_2 Utilization and Reduction Technology, Department of Thermal Engineering, Tsinghua University, Beijing 100084, China

Tairan Fu[1]
Key Laboratory for Thermal Science and Power Engineering of Ministry of Education, Beijing Key Laboratory of CO_2 Utilization and Reduction Technology, Department of Thermal Engineering, Tsinghua University, Beijing 100084, China
e-mail: trfu@mail.tsinghua.edu.cn

Qiaoqi Xu
National Research Center of Gas turbine and IGCC Technology, Department of Thermal Engineering, Tsinghua University, Beijing 100084, China

Hongde Jiang
National Research Center of Gas turbine and IGCC Technology, Department of Thermal Engineering, Tsinghua University, Beijing 100084, China

Effective Spectral Emissivity of Gas Turbine Blades for Optical Pyrometry

Turbine blade temperature measurements are important for monitoring the turbine engine performance to protect the hot components from damage due to excess temperatures. However, the reflected radiation from the blades and the surrounding environment complicate the blade temperature measurements by optical pyrometers. This study characterizes the effect of the reflected radiation on the effective spectral emissivity of a three-dimensional turbine blade in a confined turbine space for optical pyrometry temperature measurements. The effective spectral emissivity distribution on a three-dimensional blade was numerically determined for various wavelengths (0.8–15.0 μm) and actual blade surface emissivities for a specified turbine blade model. When the actual spectral emissivity of the blade surface is assumed to be 0.5, the effective spectral emissivity varies from 0.5 to 0.538 at the longer wavelength of 10.0 μm and further increases from 0.5 to 1.396 at the shorter wavelength of 0.9 μm. The results show that the effective emissivity distributions at shorter wavelengths differ greatly from those at longer wavelengths. There are also obvious differences between the effective spectral emissivity and the actual surface emissivity at shorter wavelengths. The effect of the effective emissivity on the temperature measurement accuracy, when using the optical pyrometry, was also investigated for various wavelengths (0.8–15.0 μm). The results show that the radiation reflected from the blades has less effect on the temperature measurements than on the effective emissivity, especially at the shorter wavelengths of 0.8–3.0 μm. However, the temperature measurements still need to be corrected using the effective spectral emissivity to improve the temperature calculation accuracy. This analysis provides guidelines for choosing the optimum measurement wavelengths for optical pyrometry in turbine engines. [DOI: 10.1115/1.4035732]

Keywords: turbine blades, effective emissivity, temperature, pyrometry

1 Introduction

Advanced aircraft and gas turbine engines operate at very high temperatures and pressures to increase the power, improve the fuel consumption, and lower emissions [1–5]. The hot components in the engines, such as the blades and nozzles, are exposed to high temperature and high pressure gas environments with temperatures near their melting points. Surface temperature measurements of hot engine components in these harsh thermal environments are necessary to ensure the turbine engine integrity and to protect the hot components from excessive temperatures that may damage the components.

Optical pyrometry is widely used for measuring surface temperatures or flame temperatures in industrial applications and scientific research [6–19]. The optical pyrometry has been used by Siemens, GE, Advanced Fuel Research, and other companies for temperature monitoring of turbine engines for many years since the technique is noncontactable with fast response, a wide temperature range, and long working times [20–34]. Various temperature measurement techniques have been developed based on the thermal spectral radiation intensities of the hot components in turbine engines, such as single/dual/multicolor measurements, short/long wavelength measurements, and point/field target measurements. For example, Eggert et al. [26] described a versatile high-resolution pyrometer with a spectral wavelength range of 0.4–1.2 μm and a response frequency of 1 MHz for radial turbine rotor temperature mapping at the Technical University of Berlin in conjunction with Siemens. Markham et al. [27] reported simultaneous measurements with a Siemens short wavelength infrared pyrometer and an AFR long wavelength infrared pyrometer of the temperatures in the first stage of the turbine in a Siemens V84.3 A 60 Hz 180 MW engine at the Berlin Gas Turbine Development and Manufacturing Center. Rooth and Hiemstra [28] used a dual-wavelength pyrometer to monitor the temperatures of Alstom 13E2 turbine blades with thermal barrier coatings. The temperatures obtained from short and long wavelength pyrometers (1 μm and 10 μm) differed when the blade was covered with a thermal barrier coating. Taniguchi et al. [29,30] measured the temperatures of high speed rotating turbine blades using optical pyrometers based on a PIN diode and InGaAs detectors with a 1 MHz sampling rate. The blades were the first stage turbine blades of a Kawasaki M7A-01 gas turbine and a L30A industrial gas turbine at real engine conditions. Estevadeordal and coworkers [31–34] used an NIR multicolor pyrometry system developed for DARPA to study hot particulate bursts from the combustor at various engine conditions.

The accuracies of turbine blade temperatures measured by optical pyrometers are strongly affected by various factors including: *(1) the different surface emissivities at different temperatures, surface morphologies, and compositions, (2) the thermal radiation interference from the combustion gas, (3) contamination from combustion soot deposits, (4) high blade velocities and (5) reflected radiation from the other blades and the environment*. For turbine blades with complex geometries in the confined spaces of turbine engines, the effect of the reflected radiation reaching the optical sensor often has the most significant effect on the temperature measurement accuracy. Lucia and Lanfranchi [35] developed an environment reflection model for optical pyrometry by calculating the view factors for every element on the blade and

[1]Corresponding author.

Contributed by the Heat Transfer Division of ASME for publication in the Journal of Heat Transfer. Manuscript received October 1, 2016; final manuscript received December 23, 2016; published online March 15, 2017. Assoc. Editor: Laurent Pilon.

environmental surfaces after discretization. Their model used simplified two-dimensional shapes for the turbine blades and fixed positions. Gao et al. [36,37] proposed an improved reflection model that considered the effects of the angle changes as the blade rotated. Their model was based on the blade rotational angles and positions for a simplified two-dimensional blade shape.

However, the complex three-dimensional geometries of the blades and the other hot components of the turbine combustor should be considered when analyzing the radiative transfer for optical pyrometry. The purpose of this paper is to analyze the effective spectral emissivity of a blade with consideration of the three-dimensional geometries of the turbine blades inside turbines. The effective spectral emissivity distribution is given for a three-dimensional blade at various wavelengths in a turbine combustor. Then, the effect of the effective spectral emissivity on temperature measurements using optical pyrometry is discussed. This analysis provides guidelines for accurate measurements of blade temperatures based on an effective emissivity correction for optical pyrometer measurements in turbines.

2 Turbine Blade Model

Turbine blades are subjected to very harsh environments inside turbine engines. They face high temperatures, high stresses, and vibrations which can lead to blade failures, potentially destroying the entire engine. The blade operating temperatures need to be accurately measured to avoid catastrophic damage to the turbine engine. Some temperature measurement methods have been developed using optical pyrometers for monitoring the blade temperatures. However, turbine blades are designed to optimize the aerodynamics and mass center location with complex shapes that complicate temperature measurements.

The confined space inside a turbine engine with complex blade geometries and other structures has multiple reflections between the target blade surface and other surfaces when the temperatures are measured using an optical pyrometer because the surface is not an ideal blackbody or does not have a highly absorbing coating. Therefore, the thermal radiation exclusively emitted by the blade surface, which can be directly used to determine the true blade temperatures by optical pyrometry, is difficult to measure due to the effect of the complex reflections. These multiple reflections from three-dimensional structures must be considered when optical pyrometry is used for temperature measurements.

This study used a three-dimensional turbine blade model to illustrate the issue. The object of this study was the first stage turbine blades, including 90 stator vanes and 40 rotor blades with diffuse surfaces. Due to the periodic characteristics of the structures, the model was represented by four rotor blades and two stator vanes to simplify the computations with the serial numbers of the blades and vanes as shown in Fig. 1. The turbine blades were simulated with their actual geometries. Therefore, the three-dimensional structural characteristics of the simulated blades are the same as the real blades.

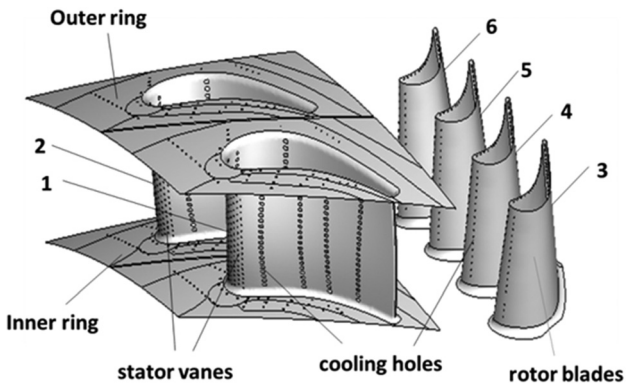

Fig. 1 Simplified model of the rotor blades and stator vanes

To investigate the effect of the reflected radiation on the optical pyrometry, the temperature distributions on the turbine blades need to be known for the analysis. Therefore, the theoretical temperature distributions on the stator vanes and the rotor blades in Fig. 1 were calculated at the desired experimental conditions by CFD simulations. The blade material was assumed to be a nickel-based high-temperature alloy with known thermal properties. The blades shown in Fig. 1 were meshed with triangular elements by ANSYS ICEM [38–40], including 46096 nodes and 84026 elements on each stator vane and 35348 nodes and 66869 elements on each rotor blade. The boundary conditions on the turbine blades were the total inlet temperature of the combustion gas $T_0 = 1420\,^{\circ}\mathrm{C}$, the total inlet pressure $P_0 = 1650\,\mathrm{kPa}$, the inlet flow angle $\alpha = 0\,^{\circ}$, and the outlet average static pressure $P_1 = 1000\,\mathrm{kPa}$. The film cooling effect due to the flow from the cooling holes shown in Fig. 1 was considered in the temperature calculations of the blade surface.

The predicted temperature distributions on the stator vanes and the rotor blades are shown in Figs. 2 and 3. The model provided the temperatures on the pressure surface and on the suction surface. The pressure surface is concave, while the suction surface is convex. For the stator vane, the highest temperature is near the blade leading edge on the pressure surface and near the blade trailing edge on the suction surface due to the direction of the combustion gas flow. In addition, the temperature distribution on the stator vane was significantly affected by the film cooling with lower temperatures around the cooling holes. The temperature distribution on the rotor blade is different from that on the stator vane. The predicted temperatures on the stator vane ranged from 449 °C to 1052 °C, while the temperatures on the rotor blade ranged from 602 °C to 1206 °C.

The turbine blade temperature calculations are not the research focus of this paper. The given blade temperature information is only given as the basis for predicting the effective emissivity and the effect of the reflected radiation. As a result, no further work was undertaken to improve the blade temperature simulation accuracy, since the conclusions of the present work are not affected by the blade temperature accuracy.

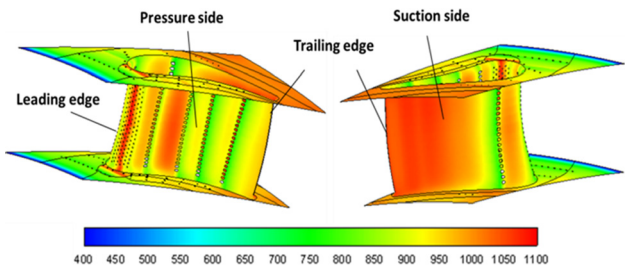

Fig. 2 Temperature distribution on the turbine stator vane with temperatures of 449–1052 °C

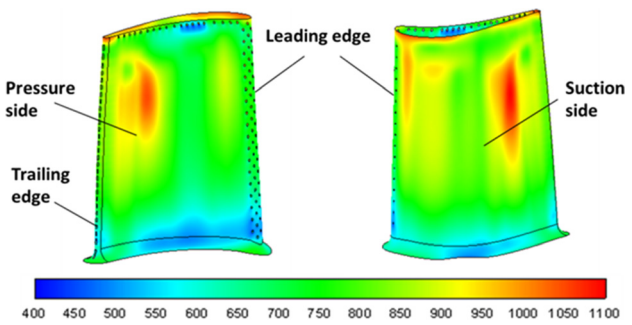

Fig. 3 Temperature distribution on the turbine rotor blade with temperatures of 602–1206 °C

3 Effective Emissivity

For the turbine blade temperature measurements by an optical pyrometer, the irradiation received by the optical pyrometer sensor, defined as the effective radiation from the target surface, contains not only the radiation emitted by the target surface, but also the radiation reflected by the target surface that originated from the curved blade surface itself, adjacent blades, and other surrounding structures. Therefore, the effective emissivity, which is the ratio of the effective radiation to the blackbody radiation at the same temperature, is an important quantity to determine the temperature from optical pyrometer measurements and will be investigated in this section.

The installation and the working conditions of the blades were such that only the reflected radiation from the same stage rotor blades and the same stage stator vanes was considered because the other reflected radiation is quite small. Due to the periodic design, the temperature distributions on each blade are approximately the same. Thus, the rotor blade #4 (Fig. 1) was chosen as the representative target for the analysis. The sketch of the measurement arrangement for rotor blade #4 is shown in Fig. 4. The three-dimensional surface of rotor blade #4 was divided into n surface units with the measured effective spectral intensity, $I_{\text{eff},i}(\lambda)$, of each surface unit, i, seen by the optical pyrometer being given by [35–37,41]

$$I_{\text{eff},i}(\lambda) = I_{\text{emit},i}(\lambda) + I_{\text{ref},i}(\lambda) = \varepsilon_i I_{\text{b}}(\lambda, T_i) + I_{\text{ref},i}(\lambda) \tag{1}$$

where $I_{\text{emit},i}(\lambda)$ is the emitted spectral intensity of surface unit i, $I_{\text{ref},i}(\lambda)$ is the reflected spectral intensity of surface unit i from the investigated blade originating from the curved blade itself and the adjacent blades, $I_{\text{b}}(\lambda, T_i)$ is the blackbody spectral intensity at the same surface unit temperature T_i, and $\varepsilon_i(\lambda)$ is the actual emissivity of surface unit i.

The reflected radiation is generally quite complex due to the complex blade geometry and the confined space. Then, considering the reflected radiation from the blade itself, the adjacent blade and the stator vane at the same stage, the reflection spectral intensity of surface unit i on rotor blade #4 can be described as [35,36]

$$I_{\text{ref},i}(\lambda) = (1-\varepsilon_i)\left(\sum_{j=1}^{n} I_{\text{eff},j}(\lambda)F_{j,i} + \sum_{k=1}^{n} I_{\text{eff},k}(\lambda)F_{k,i} + \sum_{l=1}^{m} I_{\text{eff},l}(\lambda)F_{l,i}\right) \tag{2}$$

where m is the number of surface units on the stator vane, and n is the number of the surface units on the rotor blade for the same stage. $F_{j,i}$ is the view factor from the surface unit j on blade #4 to surface unit i on blade #4, $F_{k,i}$ is the view factor from the surface unit k on blade #4 to surface unit i on blade #3, $F_{l,i}$ is the view factor from the surface unit l on blade #4 to surface unit i on vane #1, and $I_{\text{eff},j}, I_{\text{eff},k}$ and $I_{\text{eff},l}$ are the effective spectral intensities of surface units j, k, and l.

Combining Eqs. (1) and (2) gives

$$I_{\text{eff},i}(\lambda) = \varepsilon_i I_{\text{b}}(\lambda, T_i) + (1-\varepsilon_i)\left(\sum_{j=1}^{n} I_{\text{eff},j}(\lambda)F_{j,i} + \sum_{k=1}^{n} I_{\text{eff},k}(\lambda)F_{k,i} + \sum_{l=1}^{m} I_{\text{eff},l}(\lambda)F_{l,i}\right) \tag{3}$$

The surface temperature, T_i, cannot be directly determined from the measured effective spectral intensity, $I_{\text{eff},i}(\lambda)$, using a traditional optical pyrometer due to the effects of the complex reflected radiation. Therefore, the effect of the reflected radiation on the temperature measurements is found by defining an effective spectral emissivity, $\varepsilon_{\text{eff},i}$, of surface unit i based on Eq. (3)

$$\varepsilon_{\text{eff},i}(\lambda) = \frac{I_{\text{eff},i}(\lambda)}{I_{\text{b}}(\lambda, T_i)} = \varepsilon_i + \frac{(1-\varepsilon_i)}{I_{\text{b}}(\lambda, T_i)}\left(\sum_{j=1}^{n} I_{\text{eff},j}(\lambda)F_{j,i} + \sum_{k=1}^{n} I_{\text{eff},k}(\lambda)F_{k,i} + \sum_{l=1}^{m} I_{\text{eff},l}(\lambda)F_{l,i}\right) \tag{4}$$

If the effective spectral emissivity, $\varepsilon_{\text{eff},i}$, is known, the surface temperature related to $I_{\text{b}}(\lambda, T_i)$ can be determined from the effective spectral intensity, $I_{\text{eff},i}(\lambda)$. The effective spectral emissivity of surface unit i is a function of the actual surface emissivity, the blade temperature distribution, and the view factors between the surface units. Therefore, the effective spectral emissivity of the blade surface, $\varepsilon_{\text{eff},i}$, and the effective spectral intensities $(I_{\text{eff},j}, I_{\text{eff},k}, I_{\text{eff},l})$ can be found using the theoretical temperature distribution, the known actual surface emissivity and the view factors between surfaces based on Eqs. (1)–(4).

The view factor is an important parameter determining the effective spectral emissivity, that is, a function of the surface geometry. The finite-element method was used here to calculate the view factors between every surface element on the blades. Only the stator vanes and the rotor blades in the simplified three-dimensional model were considered in the view factor calculations. The blades were meshed with triangular elements by ANSYS ICEM [38–40] with 279 nodes and 437 elements on the stator vane and 196 nodes and 337 elements on the rotor blade, as shown in Fig. 4. The mesh data including the node coordinates, node numbers, surface element numbers, and the numbers of the three nodes on each triangular element were exported to TECPLOT for the calculations.

Figure 5 shows the geometric relationship between any two triangular elements for the view factor calculations. Then, the view factor between the two triangular elements is given by

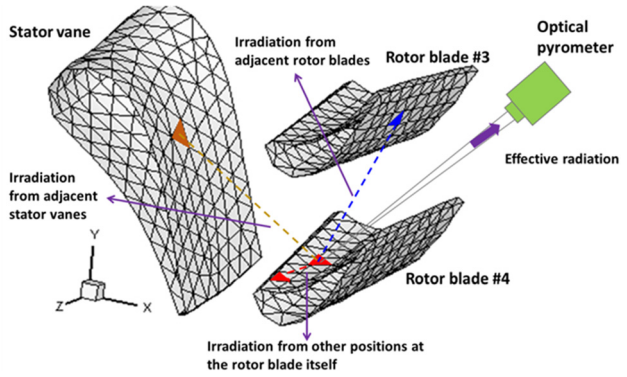

Fig. 4 Sketch of the radiation temperature measurement of blade #4 by an optical pyrometer

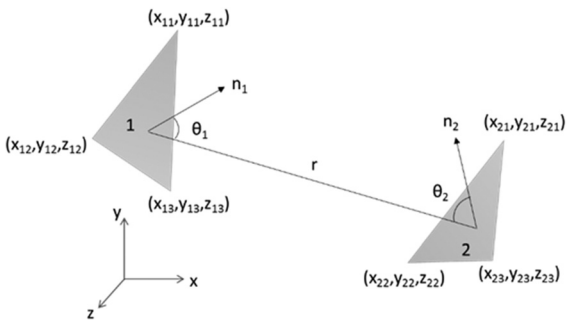

Fig. 5 View factors between two triangular elements

$$F_{\Delta_1 \to \Delta_2} = \frac{\cos\theta_1 \cos\theta_2 dA_2}{\pi r^2} \quad (5)$$

where θ_1 and θ_2 are the included angles between the normal vector and the direction vectors of triangular elements #1 and #2. A_2 is the area of element #2, and r is the length of the line connecting the centroids of triangular elements #1 and #2.

The algorithm for calculating the view factors for discrete surface elements is described here. The first step was to calculate the area and the centroid location of each triangular element using the mesh data. The surface element normals and the vectors between the centroids of each pair of triangular elements were then determined. The second step was to determine whether the triangular surface elements were visible to each other or whether a third surface lay between the two surface elements. If two triangular surface elements did not see each other, the view factor was zero. Otherwise, the view factor was calculated using Eq. (5). The third step was to verify the view factor results. The view factor calculational method used here was a general method used for radiative transfer analyses [34–36]. Once the view factors between the surfaces were determined, the effective spectral emissivity $\varepsilon_{\text{eff},i}$, of surface unit i on the blade surface was calculated using Eqs. (1)–(4), the known theoretical temperature distribution and the actual surface emissivity.

The characteristics of the effective spectral emissivity are described based on rotor blade #4 in Fig. 1. Due to the periodic structures, all the blades in each stage are similar, so that the blade choice does not affect the conclusions. The adjacent blades (#3 and #5) and vanes (#1 and #2) in the same stage are the major reflection interference sources. In the numerical analysis, the actual spectral emissivity of each blade surface was assumed to be 0.5. Then, the reflected radiation distribution and the temperatures were used to determine the effective spectral emissivity distributions on blade # 4 at various wavelengths (10.0 μm and 0.9 μm) that are shown in Figs. 6 and 7. The wavelengths 0.9 μm and 10.0 μm are generally used in commercial optical pyrometers.

The results show that the effective spectral emissivity distribution is not uniform over the blade surface even though the actual spectral emissivity is uniform. For the longer wavelength of 10.0 μm shown in Fig. 6, the effective spectral emissivity varies from 0.5 to 0.538. The maximum difference at 10.0 μm is 7.6%. Figures 3 and 6 show that the low temperature regions on the blade generally correspond to the high effective spectral emissivities since the reflected radiation more easily affects the radiation intensity measurements of the low temperature surface regions. The temperature end emissivity contours shown in Figs. 3 and 6 are not absolute since they are strongly affected by the geometry. In the middle concave region with the highest temperatures on the pressure surface, the effective spectral emissivity is 0.52. The maximum effective spectral emissivities on the pressure side are mainly near the leading edge. However, on the suction side, the maximum effective spectral emissivities are in the lower part of the middle blade region.

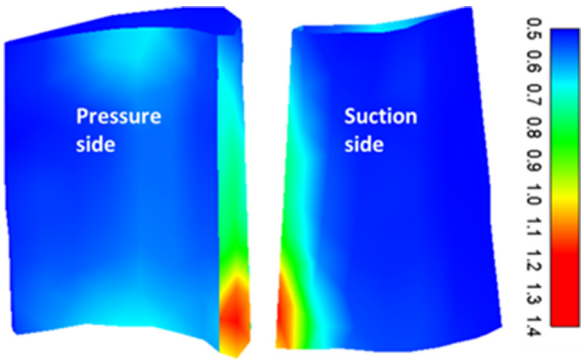

Fig. 7 Effective spectral emissivity distribution at 0.9 μm (blade #4)

Figure 7 shows the effective spectral emissivity distribution at the shorter wavelength of 0.9 μm. The effective spectral emissivity increases from 0.5 to 1.396 with a maximum increase of 179.2% at 0.9 μm. The distribution characteristics at the shorter wavelength are very different from those at the longer wavelength. The high effective spectral emissivity region (0.8–1.4) at 0.9 μm is mainly near the leading edge on the pressure and suction surfaces. The effective spectral emissivity range is (0.5, 0.7) on most of the blade except near the leading edge.

Comparison of Figs. 6 and 7 shows that the measurement wavelength used in the optical pyrometer strongly affects the effective spectral emissivity for any given blade temperature and geometry. These distribution maps of the effective spectral emissivity at various wavelengths are very useful for optical pyrometry measurement systems.

The reflected radiation in the confined measurement space strongly increases the effective spectral emissivity as shown in Figs. 6 and 7. The difference between the effective emissivity, ε_{eff}, and the actual emissivity, ε, is defined as the absolute emissivity error with the relative emissivity error, δ_ε, expressed as

$$\delta_\varepsilon = (\varepsilon_{\text{eff}} - \varepsilon)/\varepsilon \quad (6)$$

To illustrate the characteristics of the effective spectral emissivity at various wavelengths, the maximum relative emissivity errors for wavelengths of 0.8–15.0 μm are shown in Fig. 8. δ_ε dramatically decreases from 304.5% to 18.7% for increasing wavelengths of 0.8–2.0 μm; thus, the effective spectral emissivity is very sensitive to the measurement wavelength range in the short near-infrared region. δ_ε, then, gradually decreases from 18.7% to 7.5% for wavelengths of 2.0–5.0 μm and is then constant for the long-infrared wavelengths of 5.0–15.0 μm. Thus, the effective

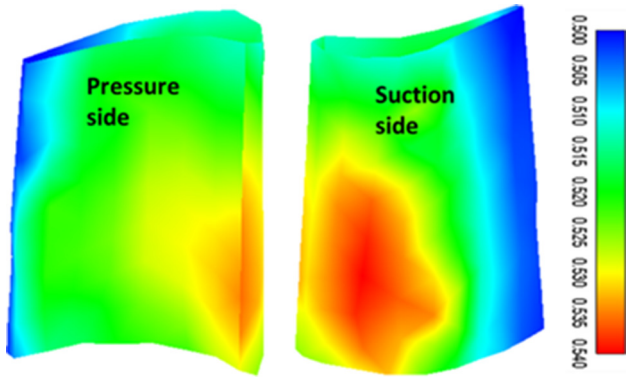

Fig. 6 Effective spectral emissivity distribution at 10.0 μm (blade #4)

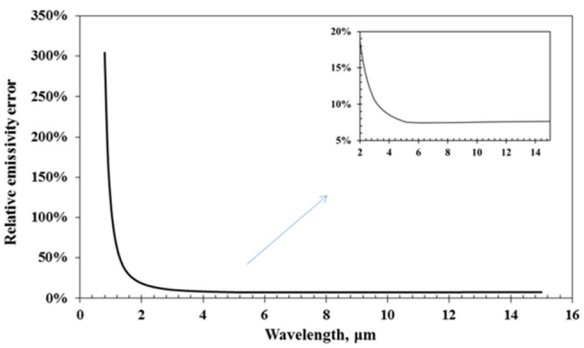

Fig. 8 Maximum relative emissivity error for wavelengths of 0.8–15 μm (rotor blade #4)

spectral emissivity is not sensitive to the wavelength in the long-infrared region.

The effect of the reflected radiation on the effective spectral emissivity differs at various wavelengths, so further investigations are needed to study the effect of the effective emissivity on the temperature measurement accuracy. Figure 9 shows that maximum relative temperature error for wavelengths of 0.8–15.0 μm obtained from the optical pyrometry measurements without the reflected radiation correction (*The effective spectral emissivity of the blade surface was instead assumed to be equal to the actual emissivity to calculate the blade temperature*). The temperature calculation error, defined as the difference between the "calculated" temperature and the true temperature, does not change linearly with the wavelength. The temperature error increases to a maximum of 8.0% at 0.8 μm and then decreases to a minimum of 2.0% with increasing wavelengths from 0.8 μm to 3.0 μm. Then, the temperature error increases from 2.0% to 5.0% with increasing wavelengths from 3.0–15.0 μm.

Comparisons of Figs. 8 and 9 illustrate the positive correlation between the temperature error and the emissivity error. The effect of this positive correlation is larger at the shorter wavelengths of 0.8–3.0 μm than at the longer wavelengths of 3.0–15.0 μm. The temperature error is much smaller than the emissivity error with emissivity errors between 10.6% and 304.5% for wavelengths of 0.8–3.0 μm, but temperature errors of only 2.0–8.0%. Thus, the reflected radiation from the blades has much less effect on the temperature measurements than on the effective spectral emissivities. However, the temperature measurements still need to be corrected using the effective spectral emissivity to improve the temperature calculation accuracy. The data in Figs. 8 and 9 are very useful for such applications. When the effective spectral emissivity is accurately known, the temperature calculated using the effective spectral emissivity correction will be significantly more accurate and will avoid the errors shown in Fig. 9. However, when the effective emissivity cannot be accurately estimated or obtained, temperature errors will exist. In this case, the measurement wavelengths should be chosen to have the smallest temperature errors with Fig. 9 as a reference to choose the optimum measurement wavelengths for optical pyrometry applications. For example, for a threshold temperature error of 3.0%, the optimum optical pyrometer wavelength should be in the range of 1.5–6.2 μm.

These numerical results need to be validated in future experiments. For a real turbine engine, the numerical results will be affected by the actual blade geometry and the experimental conditions. Although there are no available data to verify the results at present, the analysis process is reasonable and the numerical results for turbine experiments can be easily updated based on this analysis in future applications.

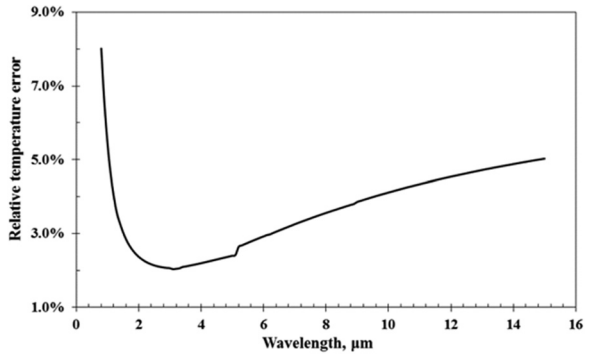

Fig. 9 Temperature errors without the reflected radiation correction for wavelengths of 0.8–15.0 μm

4 Conclusions

This study predicts the effective spectral emissivity of three-dimensional turbine blades in a confined turbine space for optical pyrometry temperature measurements to analyze the effect of the reflected radiation on the temperature measurements. The finite-element method was used to calculate the view factors between surfaces based on a discretization of the three-dimensional blade model. The effective spectral emissivity distribution on the three-dimensional blade was then determined for various wavelengths and actual surface emissivities. The results showed that the effective spectral emissivity distribution is not uniform over the blade surface even though the actual blade surface emissivity is uniform. When the actual emissivity was assumed to be 0.5, the calculated effective spectral emissivity over the blade surface at 10.0 μm varied from 0.5 to 0.538 with a maximum difference of 7.6%, while the effective emissivity at 0.9 μm increased from 0.5 to 1.396 with a maximum difference of 179.2%. Thus, the effect of the reflected radiation on the effective spectral emissivity differs at different wavelengths. The effective spectral emissivity is more sensitive to reflections at the shorter wavelengths of 0.8–2.0 μm than at the longer infrared wavelengths of 5.0–15.0 μm. There are also obvious differences between the effective spectral emissivity and the actual surface emissivity at shorter wavelengths.

The effect of the effective spectral emissivity on the temperature measurement accuracy when using an optical pyrometer was then further investigated for various wavelengths. The temperature error and the effective spectral emissivity error were larger at shorter wavelengths. The emissivity errors were quite large with errors of (10.6%, 304.5%) for wavelengths of 0.8–3.0 μm, while the temperature errors were only (2.0%, 8.0%). Thus, the radiation reflected from the blades has less effect on the temperature measurements than on the effective emissivity. However, the temperature measurements still need to be corrected using the effective spectral emissivity to improve the temperature calculation accuracy. This analysis provides a reference for choosing the optimum wavelengths for optical pyrometry systems for turbine blade temperature measurements.

5 Highlights

- Reflected radiation complicates blade temperature measurements by optical pyrometers.
- Predictions of the effective spectral emissivity of three-dimensional turbine blades.
- Effective emissivity distribution was numerically determined for various wavelengths.
- The effect of the effective emissivity on the temperature measurement accuracy was analyzed.
- The results provide reference data for optical pyrometry measurements in turbines.

Acknowledgment

This work was supported by the National Natural Science Foundation of China (Grant No. 51576110), the Science Fund for Creative Research Groups of the National Natural Science Foundation of China (Grant No. 51621062), and the Program for New Century Excellent Talents in University (Grant No. NCET-13-0315). We thank Prof. D. M. Christopher for editing the English.

Nomenclature

A_2 = area of element #2 (m^2)
$F_{j,i}$ = view factor from surface unit j to surface unit i
$F_{k,i}$ = view factor from surface unit k to surface unit i
$F_{l,i}$ = view factor from surface unit l to surface unit i
$F_{\Delta_1 \to \Delta_2}$ = view factor between two triangular elements
i, j, k, l = number indices of each surface unit

I_b = blackbody spectral intensity (W $m^{-2} sr^{-1} \mu m^{-1}$)
I_{eff} = effective spectral intensity (W $m^{-2} sr^{-1} \mu m^{-1}$)
I_{emit} = emitted spectral intensity (W $m^{-2} sr^{-1} \mu m^{-1}$)
I_{ref} = reflected spectral intensity (W $m^{-2} sr^{-1} \mu m^{-1}$)
m = number of surface units on the stator vane
n = number of surface units on the rotor blade
P_0 = total inlet pressure (kPa)
P_1 = outlet average static pressure (kPa)
r = length of the line connecting the centroids of triangular elements #1 and #2
T = surface temperature (°C)
T_0 = total combustion gas inlet temperature (°C)
α = inlet flow angle (deg)
δ_ε = relative emissivity error between the effective emissivity and the actual emissivity
ε = emissivity
λ = wavelength
θ_1, θ_2 = included angles between the normal and the direction vector of triangular elements #1 and #2

Subscripts

b = black body radiation
eff = effective radiation
emit = emitted radiation
i, j, k, l = surface unit index
ref = reflected radiation

References

[1] Li, Y. G., 2002, "Performance-Analysis-Based Gas Turbine Diagnostics: A Review," Proc. Inst. Mech. Eng., Part A, **216**(5), pp. 363–377.
[2] Poullikkas, A., 2005, "An Overview of Current and Future Sustainable Gas Turbine Technologies," Renewable and Sustainable Energy Reviews **9**(5), pp. 409–443.
[3] Wright, I. G., and Gibbons, T. B., 2007, "Recent Developments in Gas Turbine Materials and Technology and Their Implications for Syngas Firing," Int. J. Hydrogen Energy, **32**(16), pp. 3610–3621.
[4] Garg, S., 2013, "Aircraft Turbine Engine Control Research at NASA Glenn Research Center," J. Aerosp. Eng., **26**(2), pp. 422–438.
[5] Yuri, M., Masada, J., Tsukagoshi, K., Ito, E., and Hada, S., 2013, "Development of 1600 C-Class High-Efficiency Gas Turbine for Power Generation Applying J-Type Technology," Mitsubishi Heavy Ind. Tech. Rev., **50**(3), pp. 1–10.
[6] Pfefferkorn, F. E., Incropera, F. P., and Shin, Y. C., 2003, "Surface Temperature Measurement of Semi-Transparent Ceramics by Long-Wavelength Pyrometry," ASME J. Heat Transfer, **125**(1), pp. 48–56.
[7] Ranc, N., Pina, V., Sutter, G., and Philippon, S., 2004, "Temperature Measurement by Visible Pyrometry: Orthogonal Cutting Application," ASME J. Heat Transfer, **126**(6), pp. 931–936.
[8] Bendada, A., and Lamontagne, M., 2004, "A New Infrared Pyrometer for Polymer Temperature Measurement During Extrusion Moulding," Infrared Phys. Technol., **46**(1–2), pp. 11–15.
[9] Simmons, D. F., Fortgang, C. M., and Holtkamp, D. B., 2005, "Using Multispectral Imaging to Measure Temperature Profiles and Emissivity of Large Thermionic Dispenser Cathodes," Rev. Sci. Instrum., **76**(4), p. 044901.
[10] Pfänder, M., Lüpfert, E., and Heller, P., 2006, "Pyrometric Temperature Measurements on Solar Thermal High Temperature Receivers," ASME J. Sol. Energy Eng., **128**(3), pp. 285–292.
[11] Payri, F., Pastor, J. V., García, J. M., and Pastor, J. M., 2007, "Contribution to the Application of Two-Colour Imaging to Diesel Combustion," Meas. Sci. Technol., **18**(8), pp. 2579–2598.
[12] Madura, H., Kastek, M., and Piatkowski, T., 2007, "Automatic Compensation of Emissivity in Three-Wavelength Pyrometers," Infrared Phys. Technol., **51**(1), pp. 1–8.
[13] Dai, J. M., Wang, X. B., and Liu, X. D., 2008, "Peak-Wavelength Method for Temperature Measurement," Int. J. Thermophys., **29**(3), pp. 1116–1122.
[14] Densmore, J. M., Biss, M. M., McNesby, K. L., and Homan, B. E., 2011, "High-Speed Digital Color Imaging Pyrometry," Appl. Opt., **50**(17), pp. 2659–2665.
[15] Fu, T. R., Zhao, H., Zeng, J., Zhong, M. H., and Shi, C. L., 2010, "Two-Color Optical CCD-Based Pyrometer Using a Two-Peak Filter," Rev. Sci. Instrum., **81**(12), p. 124903.
[16] Fu, T. R., Yang, Z. J., Wang, L. P., Cheng, X. F., Zhong, M. H., and Shi, C. L., 2010, "Measurement Performance of Optical CCD-Based Pyrometer System," Optics Laser Tech., **42**(4), pp. 586–593.
[17] Fu, T. R., Wang, Z., and Cheng, X. F., 2010, "Temperature Measurements of a Diesel Fuel Combustion With Multicolor Pyrometry," ASME J. Heat Transfer, **132**(5), p. 051602.
[18] Fu, T. R., Tan, P., Pang, C. H., Zhao, H., and Shen, Y., 2011, "Fast Fiber-Optic Multi-Wavelength Pyrometer," Rev. Sci. Instrum., **82**(6), p. 064902.
[19] Fu, T. R., Liu, J. F., Duan, M. H., and Zong, A. Z., 2014, "Temperature Measurements Using Multicolor Pyrometry in Thermal Radiation Heating Environments," Rev. Sci. Instrum., **85**(4), p. 044901.
[20] Suarez, E., and Przirembel, H. R., 1990, "Pyrometry for Turbine Blade Development," J. Propul. Power, **6**(5), pp. 584–589.
[21] Kerr, C., and Ivey, P., 2002, "An Overview of the Measurement Errors Associated With Gas Turbine Aeroengine Pyrometer Systems," Meas. Sci. Technol., **13**(6), pp. 873–871.
[22] Kerr, C., and Ivey, P., 2004, "Optical Pyrometry for Gas Turbine Aeroengines," Sens. Rev., **24**(4), pp. 378–386.
[23] Willsch, M., Bosselmann, T., and Theune, N. M., 2004, "New Approaches for the Monitoring of Gas Turbine Blades and Vanes," IEEE Sensors Conference, Oct. 24–27, pp. 20–23.
[24] Horlock, J. H., and Torbidoni, L., 2006, "Turbine Blade Cooling: the Blade Temperature Distribution," Proc. Inst. Mech. Eng. A, **220**(4), pp. 343–353.
[25] Mori, M., Novak, L., and Sekavčnik, M., 2007, "Measurements on Rotating Blades Using IR Thermography," Exp. Therm. Fluid Sci., **32**(2), pp. 387–396.
[26] Eggert, T., Schenk, B., and Pucher, H., 2002, "Development and Evaluation of a High-Resolution Turbine Pyrometer System," ASME J. Turbomach., **124**(3), pp. 439–444.
[27] Markham, J. R., Latvakoski, H. M., Frank, S. L. F., and Lüdtke, M., 2002, "Simultaneous Short and Long Wavelength Infrared Pyrometer Measurements in a Heavy Duty Gas Turbine," ASME J. Eng. Gas Turbines Power, **124**(3), pp. 528–533.
[28] Rooth, R. A., and Hiemstra, W., 2003, "Dual Wavelength Temperature Monitoring of TBC Coated Alstom 13E2 Turbine Blades," ASME Paper No. GT2003-38814.
[29] Taniguchi, T., Sanbonsugi, K., Ozaki, Y., and Norimoto, A., 2006, "Temperature Measurement of High Speed Rotating Turbine Blades Using a Pyrometer," ASME Paper No. GT2006-90247.
[30] Taniguchi, T., Tanaka, R., Shinoda, Y., Ryu, M., Moritz, N., and Kusterer, K., 2012, "Application of an Optical Pyrometer to Newly Developed Industrial Gas Turbine," ASME Paper No. GT2012-68679.
[31] Wang, G. H., Estevadeordal, J., and Nirmalan, N., 2013, "Real-Time Multi-Color Techniques for Identification and Filtering of Burst Signals in Jet Engine Pyrometers," ASME Paper No. FEDSM 2013-16623.
[32] Estevadeordal, J., Wang, G. H., Nirmalan, N., Harper, S. P., Wang, A. Q., Lewandowski, B., and Rigney, J. D., 2012, "Multi-Color Techniques for Identification and Filtering of Burst Signals in Jet Engine Pyrometers," ASME Paper No. GT2012-69614.
[33] Estevadeordal, J., Wang, G. H., Nirmalan, N., Wang, A. Q., Harper, S. P., and Rigney, J. D., 2013, "Multicolor Techniques for Identification and Filtering of Burst Signals in Jet Engine Pyrometers," ASME J. Turbomach., **136**(3), p. 031004.
[34] Wang, G. H., Estevadeordal, J., Nirmalan, N., and Harper, S. P., 2015, "Real-Time Burst Signal Removal Using Multicolor Pyrometry Based Filter for Improved Jet Engine Control," ASME J. Turbomach., **137**(8), p. 081008.
[35] Lucia, M., and Lanfranchi, C., 1994, "An Infrared Pyrometry System for Monitoring Gas Turbine Blades: Development of a Computer Model and Experimental Results," ASME J. Eng. Gas Turbines Power, **116**(1), pp. 172–177.
[36] Gao, S., Wang, L. X., Feng, C., Xiao, Y., and Daniel, K., 2015, "Monitoring Temperature for Gas Turbine Blade: Correction of Reflection Model," Opt. Eng., **54**(6), p. 065102.
[37] Gao, S., Wang, L. X., Feng, C., and Daniel, K., 2015, "Analysis and Improvement of Gas Turbine Blade Temperature Measurement Error," Meas. Sci. Technol., **26**(10), p. 105203.
[38] Almohammadi, K. M., Ingham, D. B., Ma, L., and Pourkashan, M., 2013, "Computational Fluid Dynamics (CFD) Mesh Independency Techniques for a Straight Blade Vertical Axis Wind Turbine," Energy, **58**, pp. 483–493.
[39] Mathew, S., Ravelli, S., and Bogard, D. G., 2013, "Evaluation of CFD Predictions Using Thermal Field Measurements on a Simulated Film Cooled Turbine Blade Leading Edge," ASME J. Turbomach., **135**(1), p. 011021.
[40] Xu, L., and Luo, H., 2008, "The Technology of Numerical Simulation Based on ANSYS ICEM CFD and CFX Software," Mech. Eng., **12**, p. 049.
[41] Howell, J. R., Siegel, R., and Menguc, M. P., 2010, *Thermal Radiation Heat Transfer*, 5th ed., CRC Press, Boca Raton, FL.